Fiber orientation assessment on randomly-oriented strands composites by means of infrared thermography

Henrique Fernandes[a,*], Hai Zhang[a], Clemente Ibarra-Castanedo[a], Xavier Maldague[a]

[a] *Department of Electrical and Computer Engineering, Laval University, 1065 de la Medecine Avenue, Quebec City, G1V 0A6. Canada.*

Abstract

In this paper, an infrared thermography technique is used to assess the fiber orientation on the surface of carbon fiber-reinforced polymer (CFRP) moulded with randomly-oriented strands (ROS). Due to the randomness of the material a point by point inspection would be very time consuming. In this paper it is propose the use a flying laser spot technique to heat a line-region on the surface of the sample instead of a spot. During our experiments, a flying laser spot inspection was performed in a half of a minute while a point by point inspection of the same area would last about 25 minutes. Artificial neural network (ANN) is then used to estimate the fiber orientation over the heated line. The classification rate obtained with the network was 91.2% for the training stage and 71.6% for the testing stage.

Keywords: A. Carbon fibres, A. Randomly-oriented strands, B. Fiber orientation, D. Non-destructive testing, D. Infrared (IR) spectroscopy

1. Introduction

In the last decades composite materials (CM) has become very important in the aeronautic industry. The mass percentage of the Boeing 787 for example is more than 50% composed of composite materials (excluding the engines) [1]. One of the factors that motivates the use of CM is the fact that they are typically

*Corresponding author: henrique-coelho.fernandes.1@ulaval.ca

lighter and more resistant to corrosion than the metallic material that have been traditionally used. Fiber orientation and distribution is an important feature of fiber-reinforced composite materials (CFRP) since material's strength and stiffness are larger on the direction of the fibers. Thus it is important to assess the fiber orientation on such materials for quality control purposes. Infrared thermography enables such assessment.

Infrared thermography (IT) is a safe non-destructive testing (NDT) technique that has a fast inspection rate and is generally contactless. It is used for diagnostics and monitoring in several fields such as electrical components, thermal comfort, buildings, artworks, composite materials and others. IT popularity has grown in the recent years due to spatial resolution and acquisition rate improvements of infrared cameras while they became more affordable. Another factor is the development of advanced image processing techniques focused on this kind of image. In active IT an external heat source is used to stimulate the material being inspected in order to generate a thermal contrast between the feature of interest and the background. The active approach is adopted in many cases given that the inspected parts are usually in equilibrium with the surroundings [2].

A pulse laser heating spot technique known as Pulsed Thermal Ellipsometry (PTE) [3, 4, 5] enables the assessment of the fiber orientation of a region around a single spot. In the case of laminates which usually have an uniform fiber orientation on each ply, the inspection of two or three points with PTE would give a good indication of the fiber orientation on the surface for example. However, in the case of randomly-oriented strands (ROS) plates it is more complicated. Due to the randomness of the structure of the plate the fiber orientation on the surface would also be random and to have a good assessment of the fiber orientation distribution, several points covering all the surface should be inspected. This would prove to be very time consuming using the single spot-heating technique such as PTE. Thus, we propose in this paper a faster technique to assess the fiber orientation on the surface of a ROS plate: a flying-spot technique in combination with an artificial neural network (ANN) to assess

the fiber orientation over a line on the surface of a ROS plate.

This paper is organized as follows: the next section presents the material and methods including a brief literature review on PTE and ROS samples as well as a review on the flying spot technique used and ANNs; in section 3 results obtained are presented and in section 4 they are discussed; finally in our final considerations are presented in section 5 .

2. Material and methods

2.1. Randomly-oriented strand (ROS) material

Introduced in the late 2000s, a novel composite material called randomly-oriented unidirectional strands (ROS) composites allows the manufacturing of high performance complex parts. ROS utilizes the performance benefits of continuous fibers while sharing the advantages of processability common to short discontinuous fibers. This is illustrated schematically in Figure 1.

Conventional continuous fibers offer the mechanical performance but they are very difficult to form. On the other hand, parts with complex features can be injection moulded using lower volume content of short fibers, but they will lack mechanical properties. ROS composites lie in between these two material configuration. ROS composites are obtained from a bulk moulding compound comprised of strands of high fiber volume content unidirectional thermoplastic/thermoset pre-impregnated tape that are compression moulded with heat

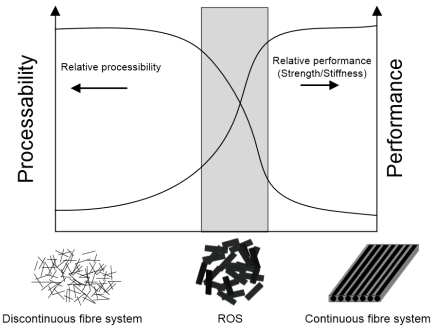

Figure 1: Processing and performance of various composite materials systems.

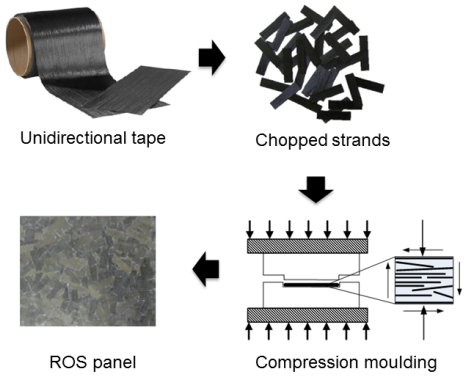

Figure 2: ROS manufacturing cycle. Adapeted from [6].

and pressure. Figure 2 depicts the manufacturing cycle of ROS composite parts by compression moulding.

CFRP panels inspected in this paper were moulded using carbon/PEEK unidirectional slit tape, which was cut into strands of 25 x 8 mm using an automated tape cutter. Strands were placed into the mould in small batches and shuffled each time to better control their distribution and to minimize their out-of-plane orientation. The mould was closed, placed into a pre-heated press and a pressure of 34 bars was applied. The mould temperature was increased up to 380°C and was maintained for 15 minutes. It was then cooled down at an approximate rate of 10°C/min and removed from the press. Panels were then cut in 100 x 100 mm samples for inspection. Figure 3 shows the three inspected samples in the scope of this research. In each sample, 4 different lines

(a) (b) (c)

Figure 3: Inspected ROS samples.

were inspected with the approach described in sub-section 2.3. Thus, a total 12 different lines (regions) were inspected.

2.2. Pulsed Thermal Ellipsometry - PTE

More than one century ago, De Senarmont [7] applied a thermal approach to determine the principal orientations in crystal plates: he covered them with a thin layer of wax, heated them over a small spot and monitored the isotherm shape revealed by the solid/liquid transition contour appearing in the wax layer. The isotherm proved to be elliptical and its aspect ratio is related to the square root of the principal conductivities in the surface plane.

Later, Krapez et al. [3, 4] applied this method (with, of course, up-to-date experimental equipment) on polymer materials to establish a correlation between their draw ratio and the induced thermal anisotropy. They referred to the method as "Thermal Ellipsometry". It was also used to evaluate the fiber orientation in the case of composite materials using short or long carbon fibers. For the latter problem, Cielo et al. presented in [8] a comparative review of a number of optical techniques for the characterization of non-metallic materials. One possibility reported by them is the evaluation of phase (or fiber) orientation in stretched polymer films or in composites by an analysis of the thermal propagation pattern. They spot-heated the inspected part by a narrow laser beam and the resulting heat-propagation pattern was analyzed by an IR camera. If the material is oriented an elliptical thermal pattern is observed, with the ratio between the two principal axes (b/a) being related to the square root of the thermal conductivities in the longitudinal and transverse directions. A test on an isotropic material would give a circle instead of an ellipse. A typical set-up used in PTE inspection is showed in Figure 4 .

Krapez conducted a detailed theoretical analysis [3] through an analytical treatment of thermal diffusion in laminates made of orthotropic layers assuming the surface is submitted to concentrated heating. Three temporal regimes were considered in that study: steady-state regime, transient regime and modulated regime (in order to analyze how the so-called thermal waves "propagate" in

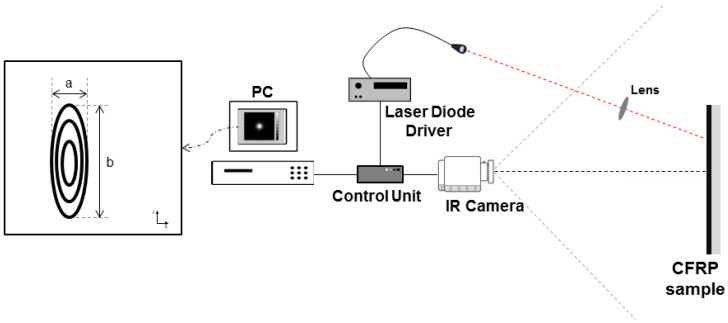

Figure 4: Pulsed Thermal Ellipsometry (PTE) schematic set-up for fiber orientation assessment in CFRP. Adapted from [9].

orthotropic laminates). Experiments were performed on carbon-epoxy laminates for all three regimes. In [4], Krapez used the same theory, i.e. thermal anisotropy measurements method which consists in analyzing the shape of the isotherms which develop around a heated spot, to develop a thermal inversion method to infer thickness of skin and core layers of a 3-layer carbon/epoxy laminate.

In our previous work [10], as in Karpen et al. [11], lock-in thermography (harmonic thermal waves) is used to probe orientation fields of carbon fibers both along the surface and in depth at low modulation frequencies and within a short time. Later Karpen et al. [12] developed a theoretical model in order to correctly interpret their measurements.

2.3. Flying laser spot

Flying laser spot is a dynamic active thermography technique, which can be employed for the inspection of materials by heating a component, point-by-point, while acquiring a series of thermograms with an infrared camera. This can be done in two ways, either the thermographic head, consisting of an infrared camera and an energy source, i.e. a CW laser source, moves along the surface while the sample to be inspected is motionless, or it may be the sample that is in motion while the thermographic head stands still. In both cases, the thermal history for every pixel can be precisely tracked by controlling the displacement speed, either the laser or the sample, and the rate of data acquisition. Detailed

theoretical and experimental aspects of this technique can be found in [13].

In this work, the approach adopted is the one which the camera and CW laser source are motionless and the inspected sample moves. For each inspection, the sample is displaced in front of the thermographic head in a way that in the first recorded image the sample does not appears in the recorded image and in the last one the sample does not appear either. In the images between the first and last one, the sample appears in different positions on each image. This displacement of the sample is performed with an aid of a robotic arm which moves the inspected sample from left to right (or right to left) in front of the camera's field of view. The use of a robotic arm provides the possibility to program the inspection path and to control the inspection speed displacement and acquisition rate in a precise manner.

In the recorded raw sequence, the sample obviously appears to be moving. In order to perform advanced image process technique, the sequence must be rearranged into a pseudo-static sequence so that the sample appears motionless. The

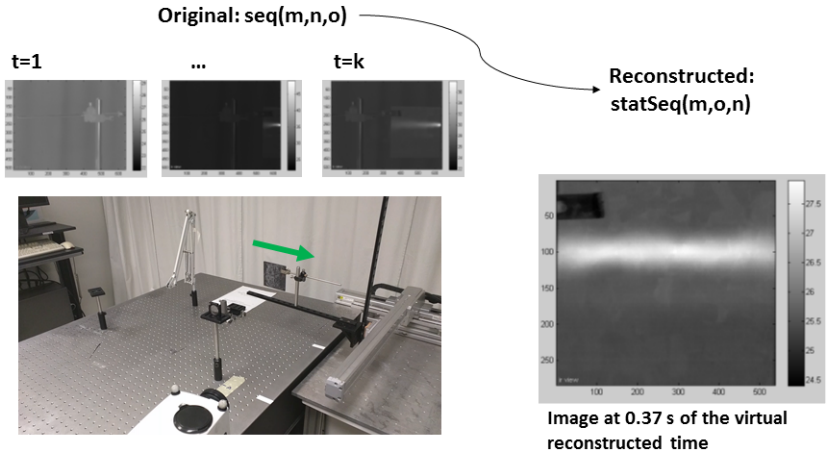

Figure 5: Pseudo-static sequence reconstruction. In the top of the figure, three images from the original sequence at different times are shown. Bellow these images, the experimental set-up is shown: the infrared camera and the inspected sample can be seen as well as the robotic-arm used to displace the sample. The green arrow indicates the sense of displacement. On the right, an image from the reconstructed pseudo-static sequence is showed.

reconstructed sequence (matrix) is obtained by following the temporal evolution of every pixel independently, in such a way that, a given pixel of the original sequence $P(x_i, y_j, t)$, is recovered frame by frame through time t and reallocated into a new image. For instance, a pixel P that is in a determined position at time t will be in a different position at a later time. Figure 5 shows some images of an original sequence and an image from the corresponding pseudo-static reconstructed sequence. Part of the experimental set-up used is also showed (the laser source is not shown). The arrow indicates the sense of the sample's movement.

2.4. Infrared image processing

After the pseudo-static sequence is obtained, principal component thermography (PCT) is applied in the reconstructed sequence. PCT, originally proposed by Rajic in[14], extracts the image features and reduces undesirable signals. It relies on singular value decomposition (SVD), which is a tool to extract spatial and temporal data from a matrix in a compact manner by projecting original data onto a system of orthogonal components known as empirical orthogonal functions (EOF).

The SVD of a MxN matrix A, where M > N, can be calculated as follows:

$$A = URV^T \tag{1}$$

where U is a MxN orthogonal matrix, R being a diagonal NxN matrix (with singular values of A present in the diagonal), V^T is the transpose of a NxN orthogonal matrix (characteristic time) as proposed in [14].

Hence, in order to apply the SVD to thermographic data, the 3D thermogram matrix representing time and spatial variations has to be reorganised as a 2D MxN matrix A. This can be done by rearranging the thermograms for every time as columns in A, in such a way that time variations will occur column-wise while spatial variations will occur row-wise. Under this configuration, the columns of U represent a set of orthogonal statistical modes known as empirical orthogonal functions (EOF) that describe the data spatial variations. On the other hand,

the principal components (PCs), which represent time variations, are arranged row-wise in matrix V^T. The first EOF will represent the most characteristic variability of the data; the second EOF will contain the second most important variability, and so on. Usually, original data can be adequately represented with only a few EOFs. Typically, an infrared sequence of 1000 images can be replaced by 10 or less EOFs.

Figure 6 shows an example of a line region (from sample showed in Figure 3a) inspected with the flying laser spot approach. The reconstructed line obtained from the flying laser spot inspection was, at early times, approximately 3 mm wide which is the same diameter as the spot that heated the sample's surface. The length of the line was 100 mm, which is the same dimension of the sample. Figure 6a shows a the region that was inspected on the surface of the sample, Figure 6b show the first EOF image, normalized between 0 and 1, obtained from the PCT application on the pseudo-static reconstructed sequence and Figure 6c shows the the binary image obtained from Figure 6b. Both the first EOF image

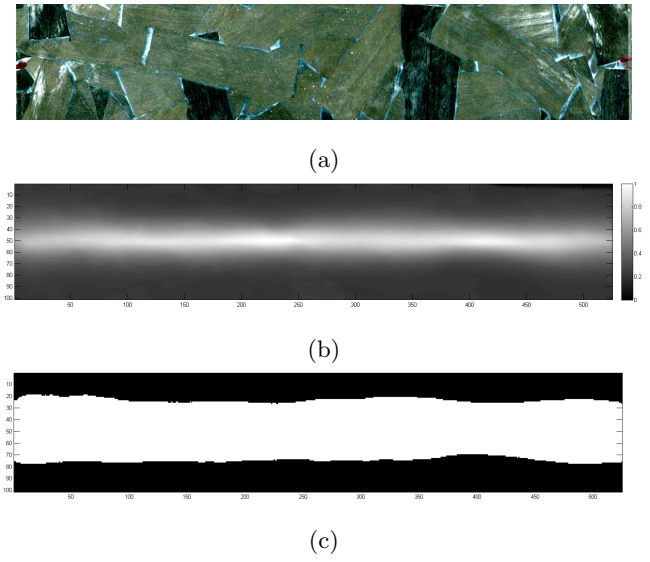

(a)

(b)

(c)

Figure 6: (a) Region on the surface of the sample inspected with the flying laser spot approach, (b) first EOF image obtained with the application of PCT on the pseudo-static reconstructed infrared sequence and (c) correspondent binary image calculated from (b).

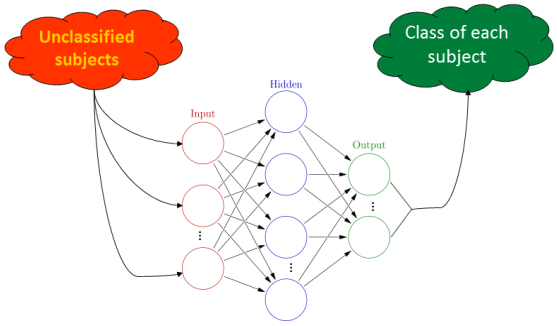

Figure 7: ANN with one hidden layer. It approximates functions that can depend on a large number of input values and are generally unknown.

and respective binary image are used in the following steps of our approach in order to assess the fiber orientation.

2.5. Artificial neural networks - ANNs

Artificial Neural Network (ANN) is an information processing paradigm that is inspired by the way biological nervous systems, such as the brain, process information. It is composed of a large number of highly interconnected processing elements (neurons) working in unison to solve specific problems. ANNs, like people, learn by example. An ANN is configured for a specific application, such as pattern recognition or data classification, through a learning process. Learning in biological systems involves adjustments to the synaptic connections that exist between the neurons. This is true of ANNs as well. Figure 7 shows how an ANN (with one hidden layer) basically works. There are several works involving ANN in the literature. A good review on image processing with ANN can be found in [15]. In infrared thermography, ANN has also been used for years for defect depth estimation [16, 17, 18, 19].

In this work, a two-layer feed-forward network, with sigmoid hidden and *softmax* output neurons trained with scaled conjugate gradient backpropagation is used to classify points on the reconstructed line obtained with the pseudo-static infrared sequence into their corresponding class (fiber orientation). Sample, i.e. points extracted from the line, are divided into three sets of samples: 70% of

the total of samples is used to train the network, 15% is used for validation during training and the remaining 15% is used for testing the network after the training has finished. Next, data representation of input samples is detailed as well as how classes are organized.

2.6. Data representation

After each one of the 12 lines were inspected and PCT applied on the reconstructed pseudo-static sequences, each of the binary EOF images were divided into 49 samples of 10 x 89 pixels each. Then, each one of these samples (588 in total) were later used to estimate the fiber orientation of each particular region. However, before estimating the fiber orientation, it is important to define the data structure to be used to represent each sample. These data is used later as input of the ANN.

The envelope of the binary line (a binary line example can be can be found in Figure 6c) is extracted and then 11 features are calculated for each sample. Figure 8 shows the envelope extracted from the image on Figure 6c. Each sample has two line segments originating from the line envelop: top and bottom line segments. These line segments belong to the edges of the binary image. The first two extracted features are the normal to the line segment orientation regarding the x-axis: θ_1 and θ_2. The next two features are the curvature values (k_1 and k_2: it is a measure of how much the curve deviates from a straight line) in the middle points of the top and bottom line segments. The fifth feature is the width of the envelope on its middle section. The last six extracted features are also related to the width of the envelop: the distance (in pixels) from the envelope's centroid to six points on the envelope edges (Figure 9 show the position of these points).

The original EOF image is divided in the same manner that the binary image was divided. Then, the pixels of each sample (from the EOF image) are rearranged line-wise. The input data of the ANN, i.e. the data used to describe each sample, is the combination of the 11 features calculated before with the line-wise pixels from the EOF image and its immediate left and right neighbors.

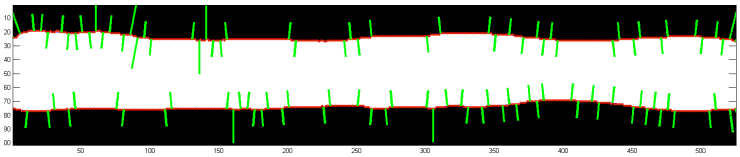

Figure 8: Line envelope. Red points represent the points that belong to the envelope and the green lines are the normal to the envelope. The magnitude of the green line represents the curvature on the point (times 300).

In total, each sample is represented by a set of 2681 numerical values. These values are the input of the network.

The output of the ANN is the class of the sample presented in the input layer. In this research, samples were classified into 4 classes. Each class covers a range of 45°. For instance, class 4 is centered at 90° and represents orientation angles ranging from 67.5° to 112.5°. Figure 10 shows an schematic example explaining how the 4 classes are divided. Thus, the output layer of the ANN has 4 neurons. Each neuron is in charge of recognizing one class, i.e. if the sample presented in the input layer belongs to first class the first neuron would has the value 1 and the other neurons value 0 (in the perfect recognition scenario). Figure 11 shows the same line showed in Figure 6 and in Figure 8 however color-coded with the target classes of each section of the line.

All 180 angles possibilities were not considered as individual classes because it would make the classification processes impossible due to the lack of information present on the line envelop that could be extracted. For instance,the distinction between an input belonging to class 15° and an input belonging to class 16° would be impossible. This point is discussed more details in section 4.

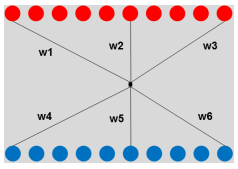

Figure 9: Line envelope width of a single sample. w1 ... w6 are the distance between the sample's centroid and six points on the envelope.

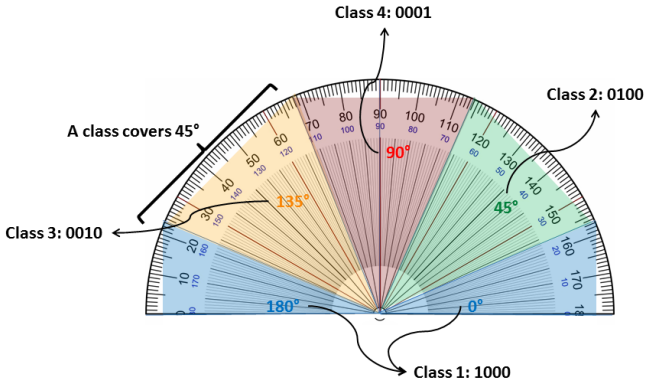

Figure 10: How recognition classes are divided. Each class covers a range of 45°.

2.7. Fiber orientation assessment

The goal of this research is to develop an approach that could estimate the fiber orientation on the surface of a ROS sample using a line heating obtained with a flying laser spot inspection. ANNs were chosen because they have the capability of estimating or approximating functions that can depend on a large number of inputs and are generally unknown which is the case. If one observes the result obtained with the PCT application on the reconstructed pseudo-static sequence (see Figure 6 and Figure 8 for instance) it can be easily observed that there is information linked to the fiber orientation on the edges of the line envelope. However, a relation between these information and the actual fiber orientation is not easily achieved. Thus, an ANN is employed.

The first step in order to employ an ANN to approximate this problem is to structure the network. In this work, a two-layer feed-forward network,

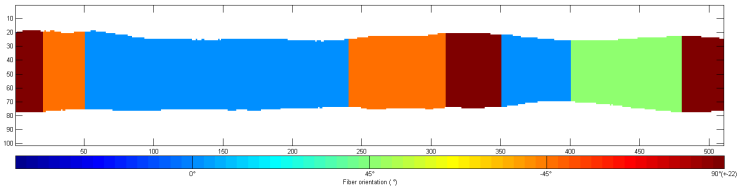

Figure 11: Inspected line color-coded with the corresponding target class. Blue is class 1, green is class 2, orange is class 3 and red is class 4.

with sigmoid hidden and *softmax* output neurons trained with scaled conjugate gradient backpropagation, is used. The input layer has 2681 neurons (one for each input value), the hidden layer has 512 neurons and the output layer has 4 neurons (one for each class).

Next, the network must be trained, i.e. the network must learn how to classify a sample. In order to train an ANN, a set of samples which the classification of each sample is known beforehand must be created. In order to create a training dataset, 49 points were previously inspected on the same region where each flying laser spot inspection would be later conducted. The same approach used in or previous work [5] was employed to assess the fiber orientation of a single point using a static laser spot heating source (or PTE, see Figure 4). Thus, 588 PTE inspections were performed in order to create a database with known orientations that are used as ground truth. From this database 412, samples were used to train the network. They were presented to the network as well as their respective classes. During the training process the network adjusts itself (its internal weights) in order to recognize the input samples presented during training into their classes with an acceptable error. From the other 176 sample, half was used for validation purpose. The other half is not presented to the network during training process and is used in order to test the network after training. Results of training and testing are presented next.

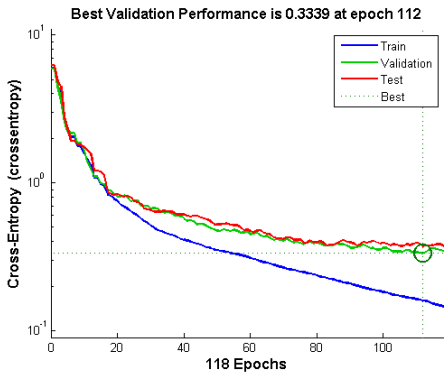

Figure 12: ANN best performance achieved during training.

3. Results

A dataset with 588 points from 12 different lines was created in order to test the proposed approach as described in the previous section. Each pseudo-static line obtained from a flying laser spot inspection was processed with PCT and divided into 49 sample of 11 x 89 pixels. 11 features were extracted from each binary image and combined with pixels values of the samples from the original EOF image obtained with PCT bringing the total of 2681 input values for each sample. 412 samples were used for training the network while 88 samples were used for validation control. The other 88 samples were later used for testing the network.

Figure 12 shows a graph with the evolution of training, validation and testing

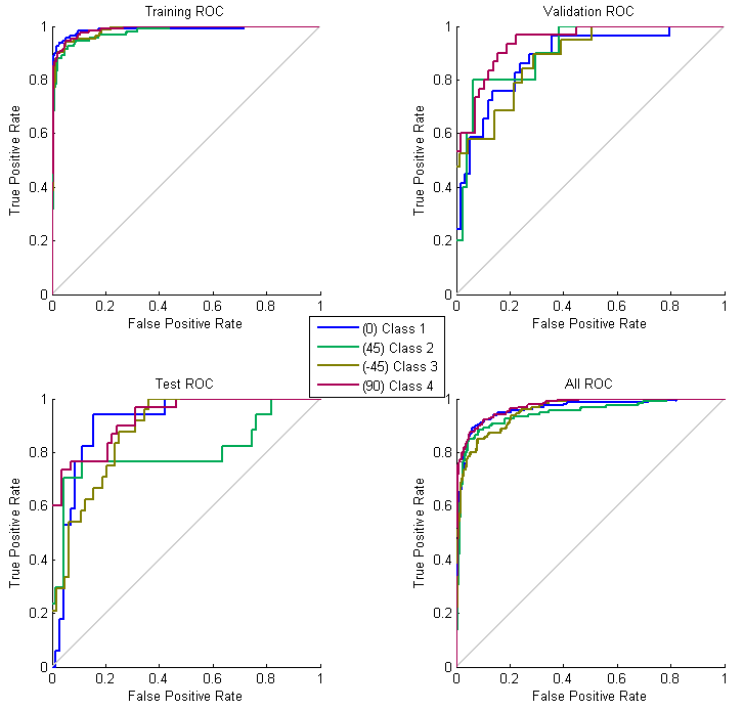

Figure 13: ROC curves.

Figure 14: Confusion matrices.

performance of the network for each epoch. The training stops after 6 epochs when no improvement was achieved in the classification of the samples in the validation group. Thus, the training stopped after 118 epochs and took about 0.58 seconds in a Matlab® environment using a PC with a 2.8 GHz Intel® i7 processor and 24 GB of RAM memory. Figure 13 shows the receiver operating characteristic curves (ROC curves) obtained for training, validation and testing. A ROC curve considering all samples is also presented. Finally, Figure 14 shows the confusion matrices, or error matrices, for each one of the sets: training, validation, testing and total.

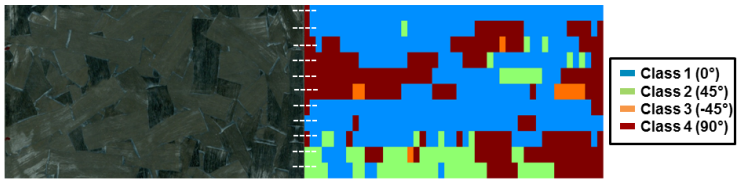

Figure 15: Results form an inspection of an unseen ROS surface. Left image is the picture of the original ROS region and the left image shows the color-coded classification performed by the ANN. Colors used are the same used in Figure 10.

Another ROS sample, which was not previously seen by the network, was tested. An region of 100 x 50 mm was inspected using the flying laser spot approach. 11 lines were inspected where the distance between each line was 5 mm. Similarly to the other tests, each line was later divided into 49 samples. Figure 15 shows the region of the sample that was inspected and the resulting color-coded classification performed by the ANN. The same colors used in Figure 10 are used here. If one visually compares the region of the sample and the classification result obtained, it can be verified the good agreement between the orientation of the strands, and consequentially the fiber, with the classification (fiber orientation) showed in the color-coded map.

4. Discussion

Accuracy obtained in the training stage was 91.3% while accuracy obtained in the testing stage was 71.6%. First, if one observes the ROC curve obtained with the testing dataset (see Figure 13) can observe that the samples of classes 2 and 3 (45° and -45°) were the ones with worst performance while sample of classes 1 and 4 (0° and 90°) performed slightly better. This suggests that the technique is having difficulties to handle samples of classes 2 and 3 however performs relatively well in the other cases.

Second, by observing the confusion matrix of all data (see Figure 14), it can be seen that the most cases of errors occurred because the network misclassified a sample into an adjacent class, i.e. sample was categorized into a class '±45°' of the class that it should be classified. For instance, the class of the sample

was 1 (0°) and the network classified it as 2 or 3 (45° and -45°) or the class of the sample was 2 (45°) and the network classified it as 1 or 4 (0° and 90°) and so on.

Third, the number of classes was limited to 4 in order to develop a first solution that could be improved later. In the current state of this research, each class is 45° wide. However, if 6 or 9 classes were used instead of 4 (30° or 20° wide respectively), the performance of the network would be severally affected. Generally, the classification rate in the testing dataset went down to 30% and 25% respectively. Nevertheless, this first results obtained with 4 classes are very promising.

Despite of its limitations, the proposed approach showed potential to assess the fiber orientation on the surface of ROS samples using a line heating region obtained with a flying laser spot. Using the proposed approach, it is possible to estimate the fiber orientation with an accuracy of 71.6%. This accuracy rate is even more acceptable when one compares the inspection time. Using the flying laser spot and ANN approach proposed in this research, the inspection time is under 30 seconds while using the classical static laser spot (PTE) inspection approach the same region would take about 25 minutes to be inspected. Moreover, the same approach was taken to assess the fiber orientaion of flat laminates with known uniform fiber orientation on the surface (0° and 90°). In this case, an accuracy rate of 100% was achieved in both training and testing. Thus, these show the great potential of proposed approach.

5. Conclusions

In this work, an approach to assess the fiber orientation on the surface of randomly-oriented strands (ROS) composite samples was presented. It uses a flying laser spot inspection technique inspired on the classical PTE (static single point) inspection technique. The proposed approach uses an artificial neural network (ANN) to estimate the fiber orientation over a line region (instead of a point) on the surface of the sample.

Tests were conducted with 3 different samples. 12 lines, 4 from each sample, were inspected with the flying laser spot technique and processed with PCT. Then, features were extracted from the obtained line to describe the changes in direction present on the edges of the line. These variations are clear related to the different fiber orientations present on the region. With these features, a ANN was used to estimate the fiber orientation of each section of each line. An accuracy of 71.6% was obtained. It is important to highlight that the inspection of the same region would take about 25 minutes with the classical PTE inspection (inspecting point by point) while using the proposed approach the same region is inspected in under 30 seconds. Thus, using the proposed technique one can easily create a surface orientation map of the fiber orientation of a ROS sample with an accuracy of 71.6% (see Figure 15).

ROS composites allow the manufacturing of high performance complex parts. There are several work available in the literature focusing on the inspection of 3D complex shaped parts [20, 21] using infrared thermography. The final goal of this research is to assess the fiber orientation on complex shaped parts manufactured with ROS material. This was done in our previous work [9] for the case of a static single point inspection (PTE). Next steps of this research include the adaptation of the proposed technique to assess fiber orientation on the surface of a complex shaped part considering its 3D complex surface and the improvement of the features used as input to the network in order to better recognize fiber orientations around 45° and -45° angles.

Acknowledments

The authors would like to gratefully acknowledge support provided by the Canada Research Chair in Multipolar Infrared Vision (MiViM) and the industrial partners: Bell Helicopter Textron Canada Limited, Bombardier Inc., Pratt and Whitney Canada Corp., Avior Integrated Products Inc., Delastek Inc. and Hutchinson Inc. Canada. The authors would also like to acknowledge the support of the following agencies: CNPq, National Council for Scientific and

Technological Development - Brazil; NSERC, Natural Sciences and Engineering Research Council of Canada; FQRNT, Quebec Fund for Research on Nature and Technology and CRIAQ, Consortium for Research and Innovation in Aerospace in Quebec. The parts tested in this work were manufactured in the Structures and Composites Materials Laboratory of McGill University and the thermography and infrared thermography inspections were conducted in the Computer Vision and Systems Laboratory of Laval University.

References

[1] J. Hale, Boeing 787, from the ground up, Aero Magazine (4) (2006) 16–23. URL http://www.boeing.com/commercial/aeromagazine/articles/qtr_4_06/article_04_2.html

[2] X. Maldague, Theory and practice of infrared technology for nondestructive testing, 1^{st} Edition, Wiley-Interscience, New York, 2001.

[3] J.-C. Krapez, Thermal ellipsometry applied to the evaluation of fibre orientation in composite, Tiré à part- Office national d'études et de recherches aerospatiales (171) (1994) 26.

[4] J.-C. Krapez, Thermal ellipsometry: A tool applied for in-depth resolved characterization of fibre orientation in composites, in: D. O. Thompson, D. E. Chimenti (Eds.), Review of Progress in Quantitative Nondestructive Evaluation, Springer US, 1996, pp. 533–540.

[5] H. C. Fernandes, X. Maldague, Fiber orientation assessment in carbon fiber reinforced composites using infrared thermography, in: S. V. Hoa, P. Hubert (Eds.), Proc. 19th International Conference on Composite Materials (Montreal, Canada, July 2013), Vol. 1, 2013, pp. 4970–4977.

[6] M. Selezneva, K. Kouwonou, L. Lessard, P. Hubert, Mechanical properties of randomly oriented strands thermoplastic composites, in: S. V. Hoa, P. Hubert (Eds.), Proc. 19th International Conference on Composite Materials (Montreal, Canada, July 2013), Vol. 1, 2013, pp. 480–488.

[7] M. H. De Senarmont, Mémoire sur la conductivité des substances cristallisées pour la chaleur: second mémoire, in: Annales de Chimie Physique, Vol. 3, 1848, pp. 179–211.

[8] P. Cielo, X. Maldague, J.-C. Krapez, R. Lewak, Optics-based techniques for the characterization of composites and ceramics, in: J. F. Bussiere, J.-P. Monchalin, C. O. Ruud, R. E. Green Jr. (Eds.), Nondestructive Characterization of Material Handbook of Technical Diagnostics, Plenum Press, 1987, pp. 733–744.

[9] H. C. Fernandes, X. Maldague, Fiber orientation assessment in complex shaped parts reinforced with carbon fiber using infrared thermography, Quantitative InfraRed Thermography Journal 12 (1) (2015) 64–79. doi:10.1080/17686733.2015.1022351.

[10] H. C. Fernandes, X. Maldague, Fiber orientation assessment on surface and beneath surface of carbon fiber reinforced composites using active infrared thermography, in: Proc. SPIE 9105, Thermosense: Thermal Infrared Applications XXXVI, Vol. 9105, International Society for Optics and Photonics, 2014, pp. 91050D–91050D–9.

[11] W. Karpen, D. Wu, R. Steegmuller, G. Busse, Depth profiling of orientation in laminates with local lock-in thermography, in: D. Balageas, G. Busse, G. Carlomagno (Eds.), Proceedings of the QIRT 94, 1994, pp. 281–286.

[12] W. Karpen, D. Wu, G. Busse, A theoretical model for the measurement of fiber orientation with thermal waves, Research in nondestructive evaluation 11 (4) (1999) 179–197.

[13] C. Gruss, D. Balageas, Theoretical and experimental applications of the flying spot camera, in: Proceedings of the QIRT 92, 1992, pp. 19–24.

[14] N. Rajic, Principal component thermography for flaw contrast enhancement and flaw depth characterisation in composite structures, Composite Structures 58 (4) (2002) 521–528.

[15] M. Egmont-Petersen, D. d. Ridder, H. Handels, Image processing with neural networks - a review, Pattern Recognition 35 (10) (2002) 2279 – 2301. doi:http://dx.doi.org/10.1016/S0031-3203(01)00178-9.

[16] X. Maldague, Y. Largouët, J.-P. Couturier, A study of defect depth using neural networks in pulsed phase thermography: modelling, noise, experiments, Revue Générale de Thermique 37 (8) (1998) 704 – 717. doi:http://dx.doi.org/10.1016/S0035-3159(98)80048-2.

[17] A. Darabi, X. Maldague, Neural network based defect detection and depth estimation in tnde, NDT& E International 35 (3) (2002) 165 – 175. doi:http://dx.doi.org/10.1016/S0963-8695(01)00041-X.

[18] H. D. Benítez, H. Loaiza, E. Caicedo, C. Ibarra-Castanedo, A. Bendada, X. Maldague, Defect characterization in infrared non-destructive testing with learning machines, NDT& E International 42 (7) (2009) 630 – 643. doi:http://dx.doi.org/10.1016/j.ndteint.2009.05.004.

[19] S. Dudzik, Characterization of material defects using active thermography and an artificial neural network, Metrology and Measurement Systems 20 (3) (2013) 491 – 500. doi:10.2478/mms-2013-0042.

[20] H. Zhang, M. Genest, F. Robitaille, X. Maldague, L. West, Joncas, C. Leduc, Infrared thermography, ultrasound c-scan and microscope for non-destructive and destructive evaluation of 3d carbon fiber materials: a comparative study, in: SPIE Sensing Technology and Applications, Vol. 9485, International Society for Optics and Photonics, 2015, p. 94850X94850X.

[21] S. Soldan, D. Ouellet, P. H. Vahid, A. H. Bendada, D. Laurendeau, A. Kroll, Mapping non-destructive testing data on the 3d geometry of objects with complex shapes, in: D. Balageas (Ed.), The 12th International Conference on Quantitative InfraRed Thermography, 7-11 July, Bordeaux, France,, 2014.